# Modified structural and functional properties of arabinoxylan derived from brewers' spent grain by ultrasound-assisted extraction

**Liwei Liu**
South China University of Technology
**Moutong Chen**
Guangdong Academy of Sciences
**Teodora Emilia Coldea**
University of Agricultural Sciences and Veterinary Medicine of Cluj-Napoca
**Huirong Yang**
Southwest Minzu University
**Haifeng Zhao** ( hfzhao@scut.edu.cn )
South China University of Technology

**Research Article**

**Keywords:** Brewers' spent grain, Arabinoxylan, Ultrasound-assisted extraction, Rheological properties, Emulsifying properties

**Posted Date:** July 5th, 2022

**DOI:** https://doi.org/10.21203/rs.3.rs-1774709/v1

# Abstract

Ultrasound-assisted extraction (UAE) was used to obtain arabinoxylan (AX) from brewers' spent grain (BSG) with a higher yield, modified structural characteristics, and improved techno-functional properties. Results showed that an UAE procedure working at 400 W for 15 min under a 60% duty cycle could increase the AX yield by 52.41% compared with a traditional alkaline extraction without sonication. Concomitantly, UAE-AX developed a degraded Mw of 2741 kDa, a changed conformation of less molecular asymmetry and a decreased mean particle size from 12.56 μm to 4.993 μm. The rheological properties of UAE-AX aqueous solution were improved, leading to higher viscosity and gel-forming capacity of the AX stabilized emulsions. As a result, UAE-AX addition could reduce the mean droplet size to 6.40 μm and better stabilize the emulsion under various conditions than traditional alkaline extracted AX. Thus, the results proved UAE to be a promising method of extracting AX from BSG with valuable utilization in food processing.


# 1. Introduction

Brewers' spent grain (BSG), one of the most abundant byproducts in beer production, is mainly composed of cellulose, hemicellulose, protein, and lignin. In BSG, arabinoxylan (AX) served as the primary hemicellulose, and was composed of xylopyranosyl residues and arabinofuranose side chains (Coelho et al. 2016). Due to its high solubility and decorated side chains, AX was regarded as a possible non-starch polysaccharide with many uses. AX has found application as an immunomodulator (Chang et al. 2021), a prebiotic (Lian et al. 2020), and an antioxidant (Ahmad 2021). Recently, various soluble polysaccharides have attracted great interest as natural emulsifiers or emulsion stabilizers. Soluble polysaccharides could form emulsions with high viscosity, gelling capacity, and pH stability, exhibiting great potential in fat substitution, encapsulation, and controlled release of bioactive compounds (Zhu 2019). As a soluble polysaccharide with a wide origin, AX had great potential in the processing of emulsions. Although AX was abundant in plant-based materials, it was often covalently bound to lignin or cellulose, and the traditional extraction was difficult to release and extract bound AX efficiently. During the malting and mashing processes used in beer production, water-extractable AX was almost wholly removed from BSG, causing the BSG-AX to be more difficult to extract.

To break the links and solubilize AX, physical, chemical, and enzymatic approaches were used alone or in combination (Zhang et al. 2014). Traditional alkaline extraction (AKE) was costly in terms of energy and low in efficiency. Ultrasound-assisted extraction (UAE) was a novel green extraction technique. The application of ultrasonic irradiation during extraction could effectively extract polysaccharides from various materials, such as mushrooms (Wang et al. 2021b), sunflower (Ezzati et al. 2020), and okra (Chen et al. 2021b). During sonication, vacuum bubbles were generated and released large amounts of energy when they collapsed, promoting the transportation of compounds and breaking covalent bonds. As a result, the extraction yield was improved. The cavitation, shearing, and steaming effects may also modify structures and affect their functionalities (Reis et al. 2015). In previous studies, the polysaccharides developed looser structures with shorter chains and higher chain flexibility (Yan et al. 2015) and had

higher antioxidant activities (Mendez-Encinas et al. 2020), bioactivities (Liu et al. 2020), and emulsifying capacities (Asgari et al. 2020) after sonication due to various structural modifications. However, the effect of ultrasound on the emulsion-stabilizing properties of AX has not been clarified yet.

Therefore, one objective of this study was to examine the extraction efficiency of ultrasounds for AX from BSG. The other objective was to clarify the changes in AX's structural and functional properties induced by sonication.

## 2. Materials And Methods

# 2.1. Materials

BSG was kindly provided by Guangzhou Zhujiang Brewery Group Co., Ltd. BSG was grinded to 0.355 mm after drying at 55 ℃ for 12 h in a hot air oven, and stored at -20 ℃ until use. All other chemicals and reagents were of analytical grade.

# 2.2. Preparation of BSG-AX

## 2.2.1. Ultrasound-assisted extraction

The ultrasound-assisted extraction procedure was modified from the earlier method (Reis et al. 2015). Briefly, pretreated BSG was first extracted in 1.5 M NaOH (1:12) using Scientz-IID ultrasonic homogenizer (Ningbo Scientz Biotechnology Co., Ltd, Ningbo, Zhejiang, China) at a frequency of 20 kHz. The power, duty cycle, and extraction time were set to 400 W, 60%, and 15 min, respectively. After extraction, the centrifuged solution was adjusted to pH = 4 with 6 M HCl, and allowed to settle overnight at 4°C to precipitate the majority of protein. The pH was then adjusted to 8.5, and 8% (w/v) $CaCl_2$ was added, then heated at 85°C for 20 min, cooled to 25°C, and centrifuged to remove the sediment. The solution was concentrated and precipitated by adding four times the volume of ethanol. Finally, the precipitant was dissolved, dialyzed, and lyophilized to obtain UAE-AX.

## 2.2.2. Traditional alkaline extraction

BSG was extracted for 4 h at 50°C in 1.5 M NaOH (1:12) and then deproteinized, precipitated, dialyzed, and lyophilized under the same conditions as UAE-AX. The product was named AKE-AX.

# 2.3. Chemical composition

## 2.3.1. Determination of composition

The protein content was determined using the Bradford method (Bradford 1976), with bovine serum albumin calibration. The total sugar content was determined using the phenol-sulfuric method (DuBois et al. 1956), with glucose as a calibration standard.

The monosaccharide analysis was performed according to previous studies (Xu et al. 2008; Coelho et al. 2016), with minor modifications. Three milligram of dried sample was first wet with 100 μL of 72% sulfuric acid and kept at room temperature for 3 h, then diluted to 2 M and boiled for 4 h. After neutralization with $Ba(OH)_2$ and adjustment to a final volume of 10 mL, the solution was centrifuged, and filtered through 0.45 μm membrane before analysis. The monosaccharide content of AX was determined by HPLC on an Agilent 1100 series HPLC (Agilent Technologies Palo, Alto, CA, USA) equipped with RID and a Hypersil $NH_2$ column (4.6 × 250 mm, Dalian Elite Analytical Instrument Co. Ltd., P.R. China). The flow rate was 1 mL/min, and the mobile phase was 80% acetonitrile aqueous solution. The injection volume was 10 μL. The column and optical unit temperatures were set at 30°C and 35°C, respectively. Different kinds of monosaccharides were dissolved in ultrapure water as standards. AX content was determined to be 90% of the total xylose and arabinose content.

## 2.3.2. GPC analysis

Before GPC analysis, samples were dissolved in 0.2 mM $K_2HPO_4$ (5 mg/mL) and filtered through a 0.22 μm membrane. GPC analysis was carried out using ACQUITY GPC system (Waters, USA) equipped with Ultrahydrogel Column (10 μm, 7.8 mm × 300 mm) and an RI detector at a flow rate of 1 mL/min using 0.2 mM $K_2HPO_4$ as the mobile phase, using β-glucans (5.2 kDa to $4.8 \times 10^3$ kDa)as standards.

# 2.4. Structure and conformation

## 2.4.1. Fourier transform infrared spectroscopy

FTIR spectrum was obtained after 2 mg of dried sample, and dry KBr (1: 100) were mixed and pressed to pellets. Every spectrum was generated after 32 scans in the range 4000–400 $cm^{-1}$.

## 2.4.2. UV spectroscopy

AX was dissolved in deionized water and diluted to a 1 mg/mL concentration. UV absorbance curve was then scanned using UV 1800 (Shimadzu, Japan) from 200 to 400 nm.

## 2.4.3. Circular dichroism (CD)

The CD measurement was conducted according to the previously reported method (Kreisman et al. 2007). AX was dissolved in deionized water, and then diluted to 0.1 mg/mL in acetonitrile aqueous solutions of different concentrations. Spectra were measured in the range of 190 nm to 350 nm using Chirascan CD spectrometer (Applied Photophysics Ltd, UK). Each sample was measured 3 times.

## 2.4.4. Dynamic light scattering

Dynamic light scattering was used to measure the mean particle size of AX in an aqueous solution. AX was dissolved in deionized water prior to the particle size (D[4,3]) were recorded by LA-960 particle size distribution analyzer (Horiba, Japan).

## 2.4.5. Scanning electronic microscopy (SEM)

After compacting the pretreated samples to the tablet and sputtering (60 s at 20 mA) with gold deposition (Quorum Technologies, UK), SEM images were obtained at an acceleration voltage of 15 kV.

## 2.5. Rheological properties

The rheological properties of AX solution were measured by HAAKE MC301 Rheometer (Thermo-Scientific, Germany) using frequency scanning mode. Shear rate was set in the range of 0.1–100 r/s, and viscosity was recorded as response. Shear rate from 0.1 Hz to 10 Hz was set as the testing range, and G' and G" were recorded to measure the viscoelasticity properties.

## 2.6. Emulsifying properties

### 2.6.1. Preparation of emulsion

AX (2%, w/v) and sodium benzoate (0.1%, w/v) were first dissolved in water to produce an aqueous phase, then the AX solution was mixed with half volume of soy oil. Emulsions were made by homogenizer for 5 min at 10000 rpm, named UAE emulsion and AKE emulsion, respectively. The emulsions were then stored at room temperature until measurements.

### 2.6.2. Particle size distribution

According to the previously reported method (Humerez-Flores et al. 2022), the measurements were performed at 20°C. The refractive index was set at 1.474 for the dispersed phase (soy oil) and 1.333 for the dispersant (water). Emulsions were diluted 50 times in deionized water before being analyzed by LA-960 particle size distribution analyzer (Horiba, Japan). The mean particle size was calculated as D[4,3] by the system.

### 2.6.3. Rheological properties

The rheological behaviors of the emulsions, including apparent viscosity and viscoelasticity, were determined before and after storage using HAAKE MC 301 Rheometer (Thermo-Scientific, Germany). The shear rate was set in the range of 0.1–100 r/s in viscosity measurements and between 0.1 Hz and 10 Hz for viscoelasticity measurements.

### 2.6.4. Thermal and freeze-thaw stabilities

The thermal and freeze-thaw stability of the emulsions were tested according to the method previously reported (Ye et al. 2021) with modifications. Briefly, the fresh emulsion was separated into 3 tubes and designated A to C. A and B were held at 4°C and − 20°C for 24 h, respectively, and then brought to 25°C in a water bath; C was heated to 90°C for 1 h and then cooled to room temperature. The emulsions were then photographed, centrifuged, and observed under a microscope.

## 2.7. Statistical analysis

All experiments were carried out in triplicate, and data were expressed as the mean ± SD. ANOVA analysis was performed at a significant difference level of $p < 0.05$ by IBM SPSS Statistic 21.0 (SPSS Inc.,

Chicago, IL, USA).

# 3. Results And Discussions

## 3.1. Chemical composition

As shown in Table 1, both UAE-AX and AKE-AX mainly consisted of polysaccharide with a minor presence of protein. A lower protein level of UAE-AX indicated the broken covalent connections between proteins and saccharides by ultrasound, as proven in previous studies (Chen et al. 2021b). Monosaccharide analysis revealed that both AXs were mainly composed of xylose, arabinose, and glucose (Table 2). No significant difference ($p < 0.05$) in the monosaccharide composition was observed. According to the previous studies on BSG-AX, xylopyranosyl residues were connected through (β 1→4), whereas arabinofuranosyl residues were mostly linked to 2/3-O of xylose through (1→2) or (1→3) (Coelho et al. 2016). Traditionally, the arabinose to xylose (A/X) ratio was employed to identify the degree of branching. The similar A/X ratios of AKE-AX (0.72) and UAE-AX (0.67) indicated a slight degradation effect on the arabinose side chains by UAE. This was in agreement with the report that the degree of branching was slightly decreased by ultrasonic degrading treatment, which suggested the cleavage of both the AX backbone and side chains (Liu et al. 2020). Also, the glucose found in AX might come from the linked or bound cellulose, as the linkages between AX and cellulose were not completely broken down either by UAE or by AKE (Coelho et al. 2016).

Table 1
Yields and contents of the main components in AKE-AX and UAE-AX

| | AKE-AX | UAE-AX |
|---|---|---|
| Yields (%) | $9.60 \pm 0.06^{b}$ | $13.60 \pm 0.17^{a}$ |
| Sugar contents (%) | $84.06 \pm 2.29^{a}$ | $85.07 \pm 3.26^{a}$ |
| Protein contents (%) | $4.04 \pm 0.19^{a}$ | $2.45 \pm 0.08^{b}$ |
| AX contents (%) | $56.20 \pm 1.34^{a}$ | $60.46 \pm 3.27^{a}$ |
| AX yields (%) | $38.37 \pm 0.91^{b}$ | $58.47 \pm 3.17^{a}$ |
| Different letters above each data indicated significant differences (Tukey test, $p < 0.05$). | | |

Table 2
Monosaccharide compositions and molecular weight of UAE-AX and AKE-AX

| | | | AKE-AX | UAE-AX |
|---|---|---|---|---|
| Monosaccharide compositions | Xylose (mol %) | | 45.77 ± 2.41[a] | 50.21 ± 6.63[a] |
| | Arabinose (mol %) | | 33.14 ± 0.87[a] | 33.62 ± 4.62[a] |
| | Glucose (mol %) | | 8.47 ± 0.92[a] | 14.52 ± 5.88[a] |
| GPC analysis | > $10^6$ kDa | Content | 8.13% | - |
| | | PDI | 14.74 | - |
| | 100–$10^5$ kDa | Content | 83.74% | 100% |
| | | PDI | 24.03 | 13.46 |
| | < 100 kDa | Content | 8.13% | - |
| | | PDI | 1.24 | - |
| Different letters above each data indicated significant differences (Tukey test, $p < 0.05$). | | | | |

GPC analysis (Table 2) showed that AKE-AX was composed of three different Mw components. The Mw of UAE-AX was decreased to 2741 kDa, the component greater than $10^6$ kDa diminished in UAE-AX, and the component between 100 kDa and $10^5$ kDa of UAE-AX also showed increased ratio and polydispersity index (PDI) than AKE-AX, implying that UAE-AX had a lower degree of polymerization but greater homogeneity due to the degradation effect of ultrasound. Previous study also reported that AX treated by ultrasonication was broken into shorter chains of a specific range of Mw (Liu et al. 2020), which was highly similar to the results observed in AXs. As previously noted by Yan et al. (Yan et al. 2015), the primary reason for the degradation was ultrasonic shearing force, the decreased PDI of AX following UAE indicated an ultrasonic degrading mechanism of midpoint scission rather than random degrading. Longer AX chains were more sensitive to shearing and therefore larger molecules over $10^6$ kDa were more easily broken than smaller ones. In addition to shortening the saccharide chains, the saccharide degradation could also increase the accessibility of side chains.

By applying UAE, total sugar yield and AX yield were improved by 43.36% and 52.41%, respectively, and the extraction time was decreased from 4 h to 15 min compared with AKE. Moreover, UAE simultaneously broke the linkages between AX and cellulose or protein, resulting in higher AX solubility and lower protein content. This demonstrated the UAE's significant potential for improving AX extraction efficiency and modifying the AX structure.

# 3.2. Structural characteristics of AXs

# 3.2.1. Ultraviolet and infrared spectrum

Figure 1 (a) depicted the UV spectra of AX extracted using two approaches, where similar peaks around 200 nm and 280 nm were observed, associated with similar composition of UAE-AX and AKE-AX. Absorption at 207 nm was attributed to n → π* transitions in saccharides (Wang et al. 2021a). The weaker absorption at 280 nm in UAE-AX was assigned to lower protein content, indicating the dissociation of AX-protein complexes induced by ultrasound, which was confirmed by the Bradford assays (Chang et al. 2021).

The FT-IR spectra of UAE-AX and AKE-AX were shown in Fig. 1 (b). The broadband around 3450 $cm^{-1}$ was attributed to the strong absorption of hydroxyl groups in the polysaccharide. The C-H stretching vibration was linked to the absorption peak at 2928 $cm^{-1}$ (Kaur et al. 2021). In addition, absorption at 1656 $cm^{-1}$ was attributed to symmetric vibration of C = O, implying the presence of carboxyl groups. Absorption at 1385 $cm^{-1}$ and 1039 $cm^{-1}$ were attributed to the vibration of C-O-C (Kaur et al. 2021), and 1426 $cm^{-1}$ was attributed to ester carbonyl groups (He et al. 2021). The absorption of β-glycosidic bond and α-glycosidic bond has been observed at 898 $cm^{-1}$ and 810 $cm^{-1}$, respectively (Jiao et al. 2021). According to Kaur et al. (2021), the absorption band from 1200 $cm^{-1}$ to 800 $cm^{-1}$ was connected to the pyranose ring in AX, and the sharp peak at 1028 $cm^{-1}$ could be a clue to a higher branched structure of AX. However, it was not prominently found in AKE-AX and UAE-AX despite their high A/X ratios. Besides, weaker absorptions at 1385 $cm^{-1}$ and 1039 $cm^{-1}$ in UAE-AX meant reduced C-O-C, thus proving the hydrolysis of saccharide and phenolic side chains after UAE.

Based on the results mentioned above, UAE-AX and AKE-AX were neutral polysaccharides containing α-glycosidic and β-glycosidic linkages, exhibiting similar characteristics in both UV and FTIR. Ultrasonication hardly affected functional groups of saccharides since most changes were observed between 1000 $cm^{-1}$ and 500 $cm^{-1}$. This was in line with the prior research indicating that ultrasonic treatment could cause degradation of polysaccharide chains but no changes in functional groups (Mendez-Encinas et al. 2020).

# 3.2.2. Circular dichroism

Circular dichroism spectroscopy was used to determine the chain conformation of AX in an aqueous solution by comparing it with reported CD spectra. As shown in Fig. 2, the presence of different characteristic peaks in UAE-AX and AKE-AX suggested that their structure in aqueous solution had changed. AKE-AX had an intense Cotton effect at 195 nm and a shoulder peak around 230 nm, while UAE-AX had a much weaker molar ellipticity than AKE-AX, with $\lambda_{min}$ observed at 215–220 nm and $\lambda_{max}$ at 200 nm. AKE-AX spectrum was assigned to the combined conformation of the random coil and β-turn (Chen et al. 2021a), while the spectrum of UAE-AX was assigned to the random coil conformation described in xanthan (Yang and Zhang 2009). The conformation of the random coil may originate from the flexibility of xylan due to the fewer hydrogen bonds, and the β-turn might come from the protein linked on AX (Picout and Ross-Murphy 2002). As the polarity gradually decreased, hydrogen bonds would be strengthened, and the molar ellipticity would be increased (Kreisman et al. 2007). However, weaker ellipticity as the polarity of the solution decreased suggested the lack of β-helix or sheet-like structures

maintained by hydrogen bonds. Decreased ellipticity and a lack of negative Cotton effect at 195 nm in UAE-AX may reflect the degradation and changed micro-environment of saccharides. Although ultrasound did not change the type of conformation, it unfolded structures and reduced asymmetry, resulting in the exposure of functional groups on UAE-AX.

### 3.2.3. Morphology

As shown in Fig. 3 (a), AKE-AX had smoother surfaces and showed “comb-like” structures, the highly ordered formations formed by the interacted chains. Contrastingly, UAE-AX exhibited more stacked and “worm-like” formations. The AKE-AX maintained more regular structures in traditional extraction process, while the UAE-AX chains were found conjugating together to form irregular structures with rough surfaces due to the destruction of the rigid structures and the improvement of chain flexibility, which was consistent with the results obtained by Wang et al. (2021b). Such changes were mainly caused by the disruption of hydrogen bonds by the shearing and cavitation effects of ultrasound. Previous study also reported increasing loose and porous structures and more fragmented pieces as the intensity of ultrasonic treatment went higher, leading to the explosive destruction of the AX physical structure (Fan et al. 2020).

### 3.2.4. Particle size

As shown in Fig. 3 (b), AKE-AX had multimodal distribution and a bigger particle size (12.56 μm), while UAE-AX had a smaller particle size (4.993 μm). The smaller particle size of UAE-AX could be explained by shorter chains after sonication. This was consistent with the results of GPC analysis that AKE-AX was composed of multiple components with different Mw, while UAE-AX had a single component, indicating that the particle size of AX molecule in solution was mainly determined by Mw. These changes in conformation and aggregated morphology after sonication could result in improved physicochemical properties and functions. As previously reported (Wu and Ma 2016), the shape and size of emulsifier particles had a significant impact on the emulsion stability. It should be noted that smaller particles not only formed emulsions with smaller droplets, but may also alter the stabilization mechanism of emulsions.

## 3.3. Rheological properties of AX solutions

### 3.3.1. Apparent viscosity

Viscosity-shear rate curves of AKE-AX and UAE-AX solutions (2%, w/v) were presented in Fig. 4 (a). Both AKE-AX (n = 0.8689, K = 0.01194) and UAE-AX (n = 0.9740, K = 0.03241) exhibited shear-thinning characteristics with decreased viscosity when subjected to high shear rates. This was the most common non-Newtonian fluid property in polymer solutions. When the shear rate increased, the entangled chains were released, and physical interactions were disrupted, resulting in a decrease in the apparent viscosity of the AX solutions. It was also found that UAE-AX had higher solution viscosity and a weaker response to the increasing shear rate. A similar effect was observed in oxidized protein, where smaller particles were found with higher viscosities and comparable gel-forming capacities (Cao et al. 2022). Such

changes could be attributed to sonication unfolding AX chains and exposing groups, as confirmed by SEM and CD. Higher chain flexibility and more exposed groups contributed to increased polysaccharide interactions and viscosities. It was reported that a more compact structure with fewer interactions could cause lower viscosity (Ye et al. 2020), which explained the UAE-AX solution having higher viscosity after sonication.

## 3.3.2. Viscoelasticity

Figure 4 (b) displayed similar viscoelastic behaviors of AKE-AX and UAE-AX solutions (2%, w/v). Both solutions showed lower loss moduli (G”) than storing moduli (G’) at low frequencies (0.01-5 Hz), indicating liquid-like behaviors, and showed greater G’ than G” at higher frequencies (5–10 Hz), indicating solid-like behavior and weak gel structures. Similar behavior was also found in *Rhododendron aganniphum* polysaccharides (Guo et al. 2017) and barley kernel arabinoxylan (Li et al. 2020). The macromolecules were able to entangle to maintain their structure and resist shearing forces. Therefore, the AX solutions exhibited solid-like behavior at high shear rates. However, a high dependency of tan δ on frequency implied that the AX molecules in the solution did not form a stable and durable gel network structure (Li et al. 2020). Although the AXs had similar viscoelastic behaviors, the higher modulus in UAE-AX demonstrated that ultrasonication might have improved the gel capacity of AX. A previous study found that the gelling capacity of arabinoxylan was improved to a certain extent after being treated with protease or dialysis. The effect was attributed to the weakening of the steric hindrance effect of the protein and the tighter group interactions of arabinoxylan (Mendez-Encinas et al. 2019). After sonication, the decreased protein content and the stronger interaction and entanglement between AX molecules caused by group exposure might be responsible for the higher gelling capacity.

# 3.4. Emulsifying capacities and stabilities

## 3.4.1. Droplet size

Microscopy images of emulsions before and after storage were shown in Fig. 5 (a). After storing for 7 days, larger and irregular droplets accompanied by flocculation of droplets were observed in AKE emulsion, while UAE emulsion showed less growth in droplet size. The oil droplets were dispersed more evenly in UAE emulsion, and there was no flocculation observed, demonstrating the greater stability and stronger liquid films on the inter-surface in UAE emulsion. Figure 5 (b) provided the size distribution of emulsions prepared freshly and stored for 7 days. After storage, D[4,3] of UAE emulsion increased from 6.40 μm to 17.27 μm, while D[4,3] of droplets in AKE emulsion increased from 21.20 μm to 32.49 μm. With more time in storage, the percentage of large droplets further increased while that of smaller droplets gradually decreased. UAE emulsion exhibited bimodal distribution after storage for 3 days, while AKE exhibited bimodal distribution right after emulsification. The particle size distribution of fresh emulsion showed a high similarity to that of AX solutions, suggesting that the initial droplet size might depend mainly on the size of emulsifier. This was in line with the conclusion that a smaller emulsifier was beneficial in reducing the oil droplet size of the emulsion. The molecular weight of AX and the particle size were reduced by UAE, and the emulsifying property was therefore improved. Shorter saccharide

chains reduced bridging, and smaller particles could more easily enter the voids between droplets and adsorb at the interface (Tang and Huang 2022). In addition, lower Mw and more flexible chains of UAE-AX also made it easier to form liquid films that covered droplets and prevented oil droplets from coalescing or liquid films from breaking apart (Ravera et al. 2021).

## 3.4.2. Rheological behavior

As shown in Fig. 5 (c), the UAE emulsion (n = 0.4612, K = 0.1561) had a higher apparent viscosity compared with the AKE emulsion (n = 0.6794, K = 0.1561). This could be attributed to the higher viscosity of the UAE-AX solution. Higher viscosity was believed to positively affect emulsion stability, as the movement rate of oil droplets in the viscous dispersed phase was reduced, and the flocculation of oil droplets was hindered (Humerez-Flores et al. 2022). After 7 days of storage, both the AKE emulsion and the UAE emulsion demonstrated reduced viscosities. An explanation of the reduced viscosities during storage might be the free polysaccharide in the initial emulsion being surrounded by oil droplets when bridging flocculation occurred, which led to the reduction of its thickening effect on the solution and emulsion (Zhai et al. 2021).

Figure 5 (d) demonstrated the viscoelastic behavior of emulsions. After storage, the storing modulus of the UAE emulsion significantly increased, the tan δ was lower than one, and the response of tan δ to frequency decreased, demonstrating the formation of a gel structure (Li et al. 2019). Although the AKE emulsion exhibited similar behavior to UAE-AX and a gel structure, the lower storage modulus indicated a weaker network. The formation of the gel structure in the emulsion resulted from the good gel-forming ability of arabinoxylan itself. The network structure formed by AX allowed the entrance of oil droplets of a specific size, forming strong gelation and inhibiting the movement of oil droplets and AXs (Ye et al. 2021). UAE-AX obtained smaller molecules and stronger interaction forces after sonication and could form a denser network in solution, wrapping and stabilizing smaller oil droplets. Wu and Ma (2016) reported that elliptical particles could effectively stabilize the emulsion. Particles with a high aspect ratio, especially rods, were beneficial to the network forming and emulsion stability, which may explain the superiority of UAE-AX in emulsion stabilization.

Conclusively, the smaller and more elliptical particles, and less asymmetric conformation may be responsible for the better emulsifying capacity of UAE-AX. The enhanced viscosity and viscoelasticity may be responsible for the higher stability of the emulsion. The higher viscosity and stronger structure constrained the droplet movement and reduced flocculation, which resulted in less aqueous solution separation from the gel structure (Huc-Mathis et al. 2021).

## 3.4.3. Stabilities against heat and freeze-thaw

Different temperatures and processing conditions were unavoidable during manufacturing, and emulsion stability should be considered in a variety of environments. Appearance and microscope images of emulsions stored at various temperatures are depicted in Fig. 6. As expected, storage in the refrigerator had the least damaging effect on emulsions, and neither AKE nor UAE emulsions exhibited visible separation. After heating, the UAE emulsion exhibited less phase separation than the AKE emulsion, and

the droplet size remained after treatment, suggesting improved heat resistance of UAE emulsion. However, severe destabilization occurred when the emulsion was subjected to freeze-thaw treatment, manifested as oiling-off and serum separation. Microscopy photos of the emulsion also revealed severe flocculation in the mass, indicating no increase in stability against freeze-thaw. Heating destroyed the emulsion mostly by accelerating the thermal motions and enhancing the droplet collisions, while higher viscosity restricted the accelerated movements of droplets caused by heating and could therefore improve the heat resistance. A possible mechanism for emulsion destabilization during freeze-thaw involved the denaturation of surfactant polymers and the destruction of droplet surfaces (Supratim and John 2008). The AX layer that covered the droplets could be destroyed after freezing due to the concentration effect or generation of ice crystals. It was reported that the anti-freeze capacity was linked to molecular weight and A/X ratio (Zhao et al. 2022), neither of which was increased in UAE-AX. This may explain the lack of improvement on anti-freeze activity of the UAE emulsion.

# 4. Conclusions

The present study clearly demonstrated that UAE could simultaneously extract and modify brewers' spent grain arabinoxylan with satisfying emulsifying capacity in a short extraction time. The structural analysis demonstrated that UAE-AX had degraded smaller particles and decreased asymmetry, which was caused by destruction of intermolecular interaction. The changed chain conformation and smaller particles led to improved rheological properties and greater emulsifying capacity of the UAE-AX. Consequently, the UAE-AX stabilized emulsion exhibited higher viscosity, gelling capacity, and enhanced stability. The research found the great potential of ultrasonic treatment in polysaccharide extraction and structural modification, which allowed UAE effective in the reuse of BSG-AX. Further study should be taken to improve the functional properties of UAE-AX to meet the needs of practical applications.

# Declarations

Acknowledgements

The authors wish to acknowledge the supports from the Science and Technology Project of Guangzhou (201903010056), the National Natural Science Foundation of China (Nos. 31972062 and 32001675), the Science and Technology Project of Guangdong Province (2018A050506008), the 111 Project (B17018), and State Key Laboratory of Applied Microbiology Southern China (SKLAM010-2021).

Ethics approval and consent to participate

Not applicable.

Consent for publication

Not applicable.

Availability of data and materials

All data generated or analyzed during this study are included in this published article.

Competing Interest

The authors declare that they have no known competing financial interests or personal relationships that could appeared to influence the work reported in this paper.

Funding

This work was supported by the Science and Technology Project of Guangzhou (201903010056), the National Natural Science Foundation of China (Nos. 31972062 and 32001675), the Science and Technology Project of Guangdong Province (2018A050506008), the 111 Project (B17018), and State Key Laboratory of Applied Microbiology Southern China (SKLAM010-2021).

Authors' Contributions

**Liwei Liu:** Conceptualization, Methodology, Writing–original draft, Data curation. **Moutong Chen:** Formal analysis, Methodology. **Teodora Emilia Coldea:** Writing–review & editing. **Huirong Yang:** Data curation, Software. **Haifeng Zhao:** Project supervision and advice.

# References

1. Ahmad M M (2021). Recent trends in chemical modification and antioxidant activities of plants-based polysaccharides: A review. Carbohydrate Polymer Technologies and Applications, 2: 100045. https://doi.org/10.1016/j.carpta.2021.100045
2. Asgari K, Labbafi M, Khodaiyan F, Kazemi M, Hosseini S S (2020). High-methylated pectin from walnut processing wastes as a potential resource: Ultrasound assisted extraction and physicochemical, structural and functional analysis. International Journal of Biological Macromolecules, 152: 1274–1282. https://doi.org/10.1016/j.ijbiomac.2019.10.224
3. Bradford M M (1976). A rapid and sensitive method for the quantitation of microgram quantities of protein utilizing the principle of protein-dye binding. Analytical Biochemistry, 72(1–2): 248–254. https://doi.org/10.1016/0003-2697(76)90527-3
4. Cao Y, Li Z, Li B, Fan X, Liu M, Zhao J (2022). Mitigation of oxidation-induced loss of myofibrillar protein gelling potential by the combination of pyrophosphate and l-lysine. Lwt, 157: 113068. https://doi.org/10.1016/j.lwt.2022.113068
5. Chang X, Shen C-Y, Jiang J-G (2021). Structural characterization of novel arabinoxylan and galactoarabinan from citron with potential antitumor and immunostimulatory activities. Carbohydrate Polymers, 269: 118331. https://doi.org/10.1016/j.carbpol.2021.118331
6. Chen X, Zhao Y, Zhao Y, Hu Y, Wang C, Zhang K, Wang C, Wu Z (2021a). Effect of ultra-high pressure treatment on the characteristics of a tea polysaccharide conjugate aqueous solution. Industrial

Crops and Products, 171: 113859. https://doi.org/10.1016/j.indcrop.2021.113859

7. Chen Z-L, Wang C, Ma H, Ma Y, Yan J-K (2021b). Physicochemical and functional characteristics of polysaccharides from okra extracted by using ultrasound at different frequencies. Food Chemistry, 361: 130138. https://doi.org/10.1016/j.foodchem.2021.130138
8. Coelho E, Rocha M a M, Moreira A S P, Domingues M R M, Coimbra M A (2016). Revisiting the structural features of arabinoxylans from brewers' spent grain. Carbohydrate Polymers, 139: 167–176. https://doi.org/10.1016/j.carbpol.2015.12.006
9. Dubois M, Gilles K A, Hamilton J K, Rebers P A, Smith F (1956). Colorimetric method for determination of sugars and related substances. Analytical Chemistry, 28(3): 350–356. https://doi.org/10.1021/ac60111a017
10. Ezzati S, Ayaseh A, Ghanbarzadeh B, Heshmati M K (2020). Pectin from sunflower by-product: Optimization of ultrasound-assisted extraction, characterization, and functional analysis. International Journal of Biological Macromolecules, 165: 776–786. https://doi.org/10.1016/j.ijbiomac.2020.09.205
11. Fan X, Chang H, Lin Y, Zhao X, Zhang A, Li S, Feng Z, Chen X (2020). Effects of ultrasound-assisted enzyme hydrolysis on the microstructure and physicochemical properties of okara fibers. Ultrasonics Sonochemistry, 69: 105247. https://doi.org/10.1016/j.ultsonch.2020.105247
12. Guo X, Shang X, Zhou X, Zhao B, Zhang J (2017). Ultrasound-assisted extraction of polysaccharides from Rhododendron aganniphum: Antioxidant activity and rheological properties. Ultrasonics Sonochemistry, 38: 246–255. https://doi.org/10.1016/j.ultsonch.2017.03.021
13. He Y, Peng H, Zhang H, Liu Y, Sun H (2021). Structural characteristics and immunopotentiation activity of two polysaccharides from the petal of Crocus sativus International Journal of Biological Macromolecules, 180: 129–142. https://doi.org/10.1016/j.ijbiomac.2021.03.006
14. Huc-Mathis D, Almeida G, Michon C (2021). Pickering emulsions based on food byproducts: A comprehensive study of soluble and insoluble contents. Journal of Colloid and Interface Science, 581: 226–237. https://doi.org/10.1016/j.jcis.2020.07.078
15. Humerez-Flores J N, Verkempinck S H E, De Bie M, Kyomugasho C, Van Loey A M, Moldenaers P, Hendrickx M E (2022). Understanding the impact of diverse structural properties of homogalacturonan rich citrus pectin-derived compounds on their emulsifying and emulsion stabilizing potential. Food Hydrocolloids, 125: 107343. https://doi.org/10.1016/j.foodhyd.2021.107343
16. Jiao L, Li J, Liu F, Wang J, Jiang P, Li B, Li H, Chen C, Wu W (2021). Characterisation, chain conformation and antifatigue effect of steamed Ginseng polysaccharides with different molecular weight. Frontiers in Pharmacology, 12: 712836. https://doi.org/10.3389/fphar.2021.712836
17. Kaur A, Singh B, Yadav M P, Bhinder S, Singh N (2021). Isolation of arabinoxylan and cellulose-rich arabinoxylan from wheat bran of different varieties and their functionalities. Food Hydrocolloids, 112: 106287. https://doi.org/10.1016/j.foodhyd.2020.106287

18. Kreisman L S C, Friedman J H, Neaga A, Cobb B A (2007). Structure and function relations with a T-cell-activating polysaccharide antigen using circular dichroism. Glycobiology, 17(1): 46–55. https://doi.org/10.1093/glycob/cwl056
19. Li L-Y, Wang Y-X, Zhang T, Zhang J-F, Pan M, Huang X-J, Yin J-Y, Nie S-P (2020). Structural characteristics and rheological properties of alkali-extracted arabinoxylan from dehulled barley kernel. Carbohydrate Polymers, 249: 116813. https://doi.org/10.1016/j.carbpol.2020.116813
20. Li X, Li J, Kuang Y, Guo S, Mo L, Ni Y (2019). Stabilization of Pickering emulsions with cellulose nanofibers derived from oil palm fruit bunch. Cellulose, 27(2): 839–851. https://doi.org/10.1007/s10570-019-02803-4
21. Lian Z, Wang Y, Luo J, Lai C, Yong Q, Yu S (2020). An integrated process to produce prebiotic xylooligosaccharides by autohydrolysis, nanofiltration and endo-xylanase from alkali-extracted xylan. Bioresource Technology, 314: 123685. https://doi.org/10.1016/j.biortech.2020.123685
22. Liu Y, Wang S, Kang J, Wang N, Xiao M, Li Z, Wang C, Guo Q, Hu X (2020). Arabinoxylan from wheat bran: molecular degradation and functional investigation. Food Hydrocolloids, 107: 105914. https://doi.org/10.1016/j.foodhyd.2020.105914
23. Mendez-Encinas M A, Carvajal-Millan E, Ortega-García J, Santiago-Gómez L B, De Anda-Flores Y, Martínez-Robinson K G, Valencia-Rivera D E (2020). Effect of ultrasound-treated arabinoxylans on the oxidative stability of soybean oil. Antioxidants, 9(2): 147. https://doi.org/10.3390/antiox9020147
24. Mendez-Encinas M A, Carvajal-Millan E, Yadav M P, López-Franco Y L, Rascon-Chu A, Lizardi-Mendoza J, Brown-Bojorquez F, Silva-Campa E, Pedroza-Montero M (2019). Partial removal of protein associated with arabinoxylans: Impact on the viscoelasticity, crosslinking content, and microstructure of the gels formed. Journal of Applied Polymer Science, 136(15): 47300. https://doi.org/10.1002/app.47300
25. Picout D R, Ross-Murphy S B (2002). On the chain flexibility of arabinoxylans and other β-(1→4) polysaccharides. Carbohydrate Research, 337(19): 1781–1784. https://doi.org/10.1016/S0008-6215(02)00281-1
26. Ravera F, Dziza K, Santini E, Cristofolini L, Liggieri L (2021). Emulsification and emulsion stability: The role of the interfacial properties. Advances in Colloid and Interface Science, 288: 102344. https://doi.org/10.1016/j.cis.2020.102344
27. Reis S F, Coelho E, Coimbra M A, Abu-Ghannam N (2015). Improved efficiency of brewer's spent grain arabinoxylans by ultrasound-assisted extraction. Ultrasonics Sonochemistry, 24: 155–164. https://doi.org/10.1016/j.ultsonch.2014.10.010
28. Supratim G, John N C (2008). Factors affecting the freeze–thaw stability of emulsions. Food Hydrocolloids, 22(1): 105–111. https://doi.org/10.1016/j.foodhyd.2007.04.013
29. Tang Q, Huang G (2022). Improving method, properties and application of polysaccharide as emulsifier. Food Chemistry, 376: 131937. https://doi.org/10.1016/j.foodchem.2021.131937
30. Wang H, Chen J, Ren P, Zhang Y, Omondi Onyango S (2021a). Ultrasound irradiation alters the spatial structure and improves the antioxidant activity of the yellow tea polysaccharide. Ultrasonics

Sonochemistry, 70: 105355. https://doi.org/10.1016/j.ultsonch.2020.105355

31. Wang K, Guo J, Cheng J, Zhao X, Ma B, Yang X, Shao H (2021b). Ultrasound-assisted extraction of polysaccharide from spent Lentinus edodes substrate: Process optimization, precipitation, structural characterization and antioxidant activity. International Journal of Biological Macromolecules, 191: 1038–1045. https://doi.org/10.1016/j.ijbiomac.2021.09.174
32. Wu J, Ma G-H (2016). Recent studies of pickering emulsions: Particles make the difference. Small, 12(34): 4633–4648. https://doi.org/10.1002/smll.201600877
33. Xu D-J, Xia Q, Wang J-J, Wang P-P (2008). Molecular weight and monosaccharide composition of Astragalus polysaccharides. Molecules, 13(10): 2408–2415. https://doi.org/10.3390/molecules13102408
34. Yan J-K, Pei J-J, Ma H-L, Wang Z-B (2015). Effects of ultrasound on molecular properties, structure, chain conformation and degradation kinetics of carboxylic curdlan. Carbohydrate Polymers, 121: 64–70. https://doi.org/10.1016/j.carbpol.2014.11.066
35. Yang L, Zhang L-M (2009). Chemical structural and chain conformational characterization of some bioactive polysaccharides isolated from natural sources. Carbohydrate Polymers, 76(3): 349–361. https://doi.org/10.1016/j.carbpol.2008.12.015
36. Ye J, Hua X, Zhang W, Zhao W, Yang R (2021). Emulsifying capacity of peanut polysaccharide: Improving interfacial property through the co-dissolution of protein during extraction. Carbohydrate Polymers, 273: 118614. https://doi.org/10.1016/j.carbpol.2021.118614
37. Ye J, Hua X, Zhao Q, Zhao W, Chu G, Zhang W, Yang R (2020). Chain conformation and rheological properties of an acid-extracted polysaccharide from peanut sediment of aqueous extraction process. Carbohydrate Polymers, 228: 115410. https://doi.org/10.1016/j.carbpol.2019.115410
38. Zhai H, Gunness P, Gidley M J (2021). Depletion and bridging flocculation of oil droplets in the presence of β-glucan, arabinoxylan and pectin polymers: Effects on lipolysis. Carbohydrate Polymers, 255: 117491. https://doi.org/10.1016/j.carbpol.2020.117491
39. Zhang Z, Smith C, Li W (2014). Extraction and modification technology of arabinoxylans from cereal by-products: A critical review. Food Research International, 65: 423–436. https://doi.org/10.1016/j.foodres.2014.05.068
40. Zhao A, Shi P, Yang R, Gu Z, Jiang D, Wang P (2022). Isolation of novel wheat bran antifreeze polysaccharides and the cryoprotective effect on frozen dough quality. Food Hydrocolloids, 125: 107446. https://doi.org/10.1016/j.foodhyd.2021.107446
41. Zhu F (2019). Starch based Pickering emulsions: Fabrication, properties, and applications. Trends in Food Science & Technology, 85: 129–137. https://doi.org/https://doi.org/10.1016/j.tifs.2019.01.012

# Figures

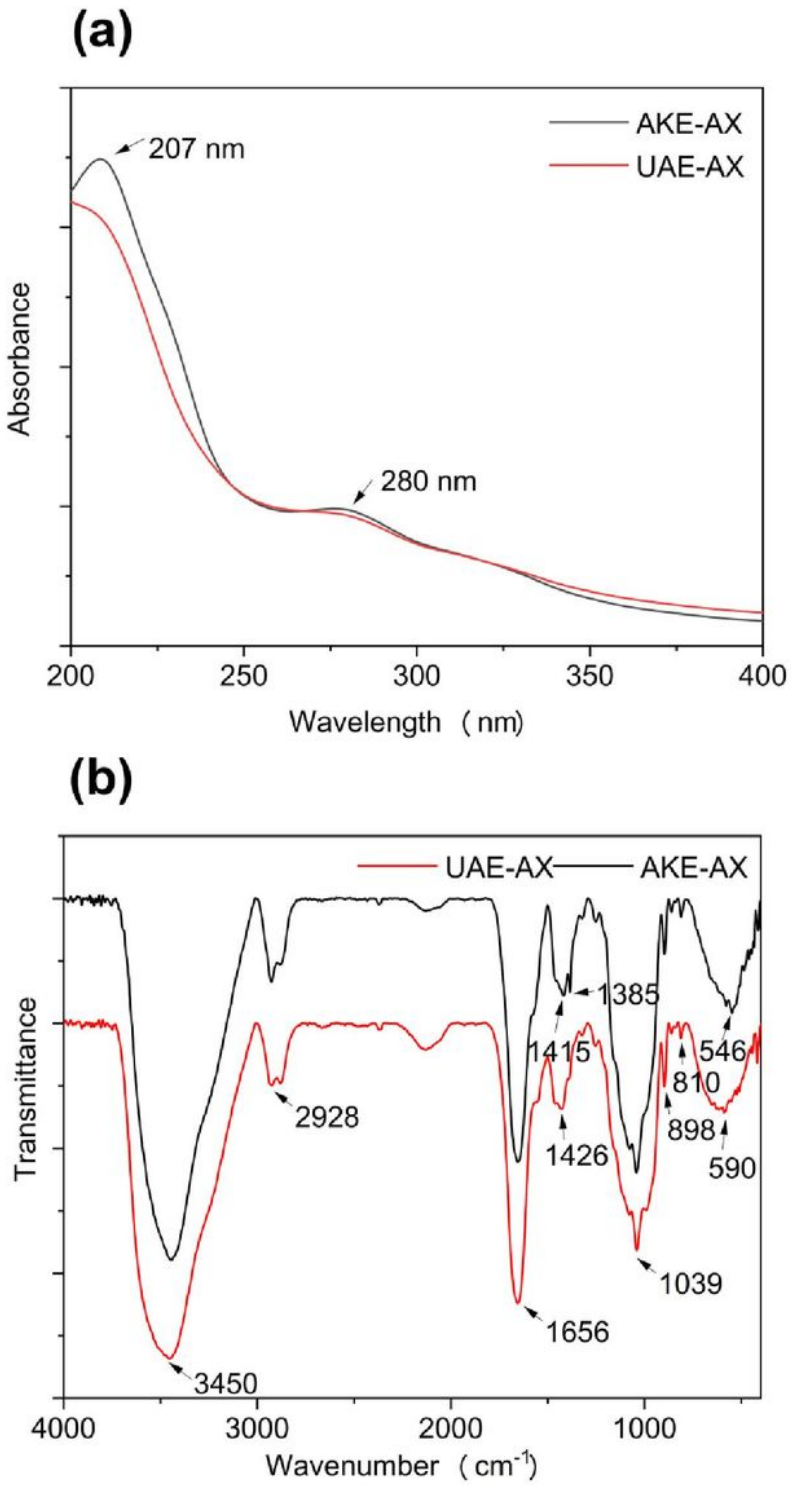


**Figure 1**

Ultraviolet spectra (a) and FTIR spectra (b) of UAE-AX and AKE-AX

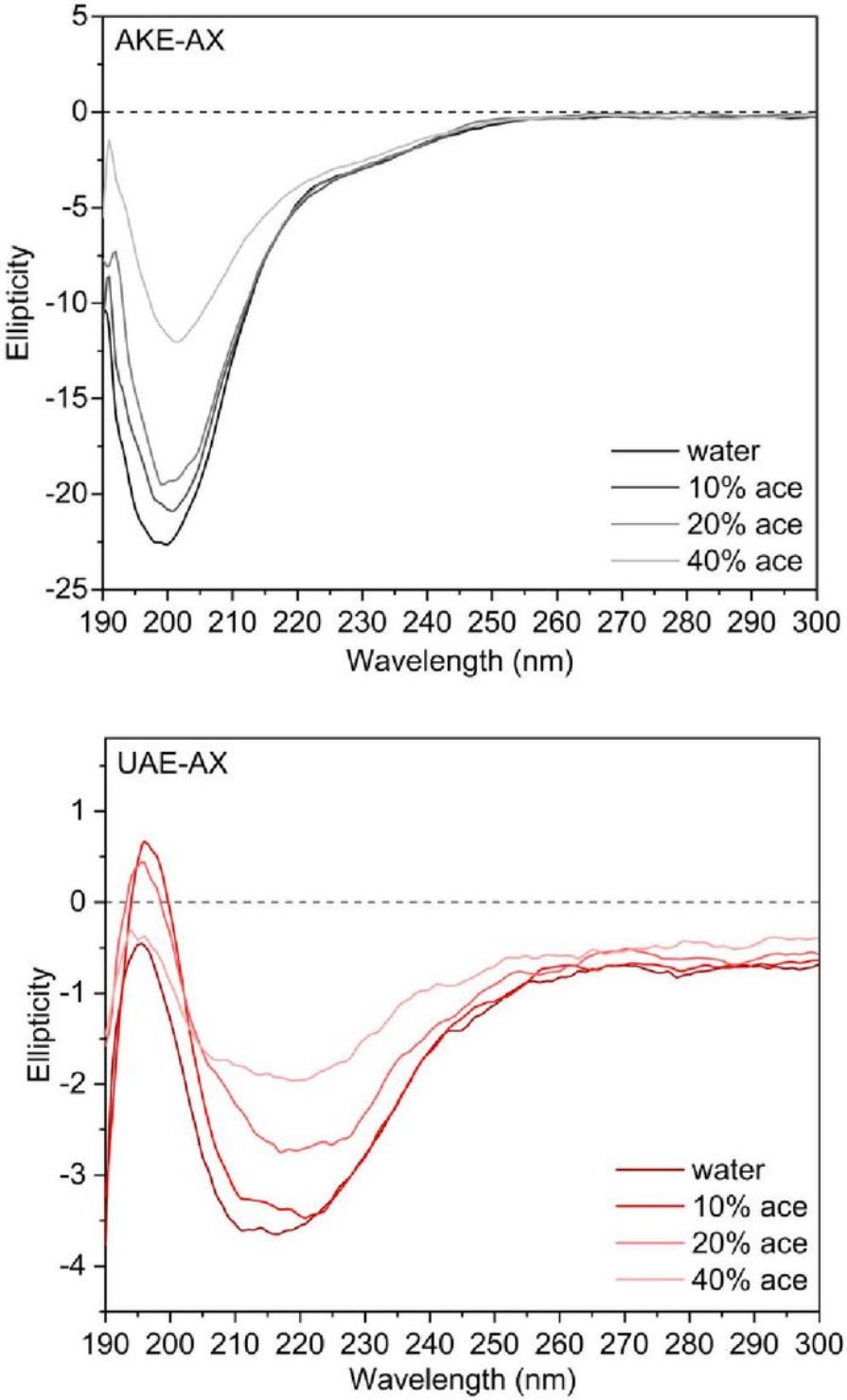


## Figure 2

Circular dichroism spectrum of AKE-AX and UAE-AX in water, 10%, 20% and 40% aqueous acetonitrile solution (v/v)

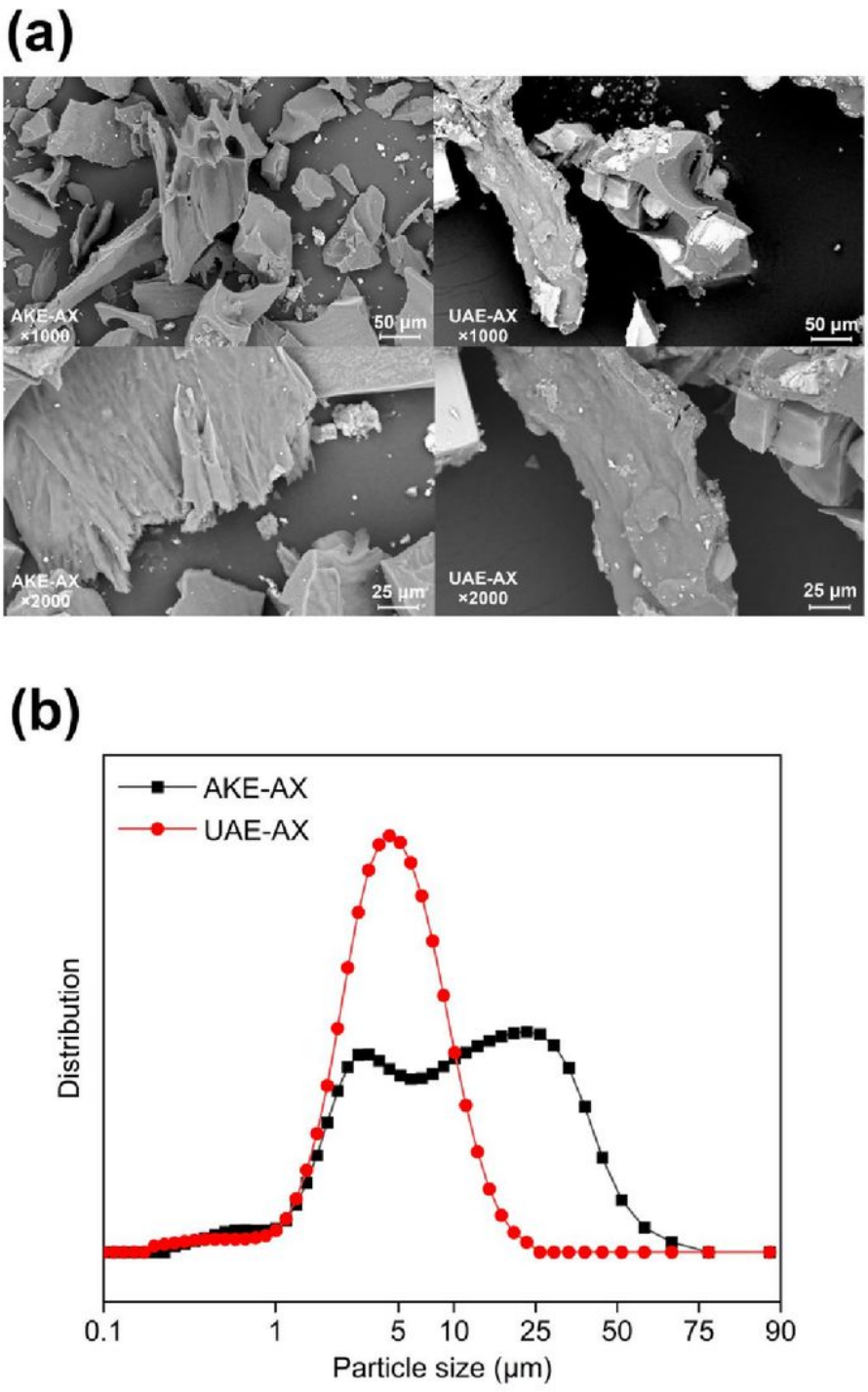


## Figure 3

(a) SEM images and (b) particle size distribution of AKE-AX and UAE-AX

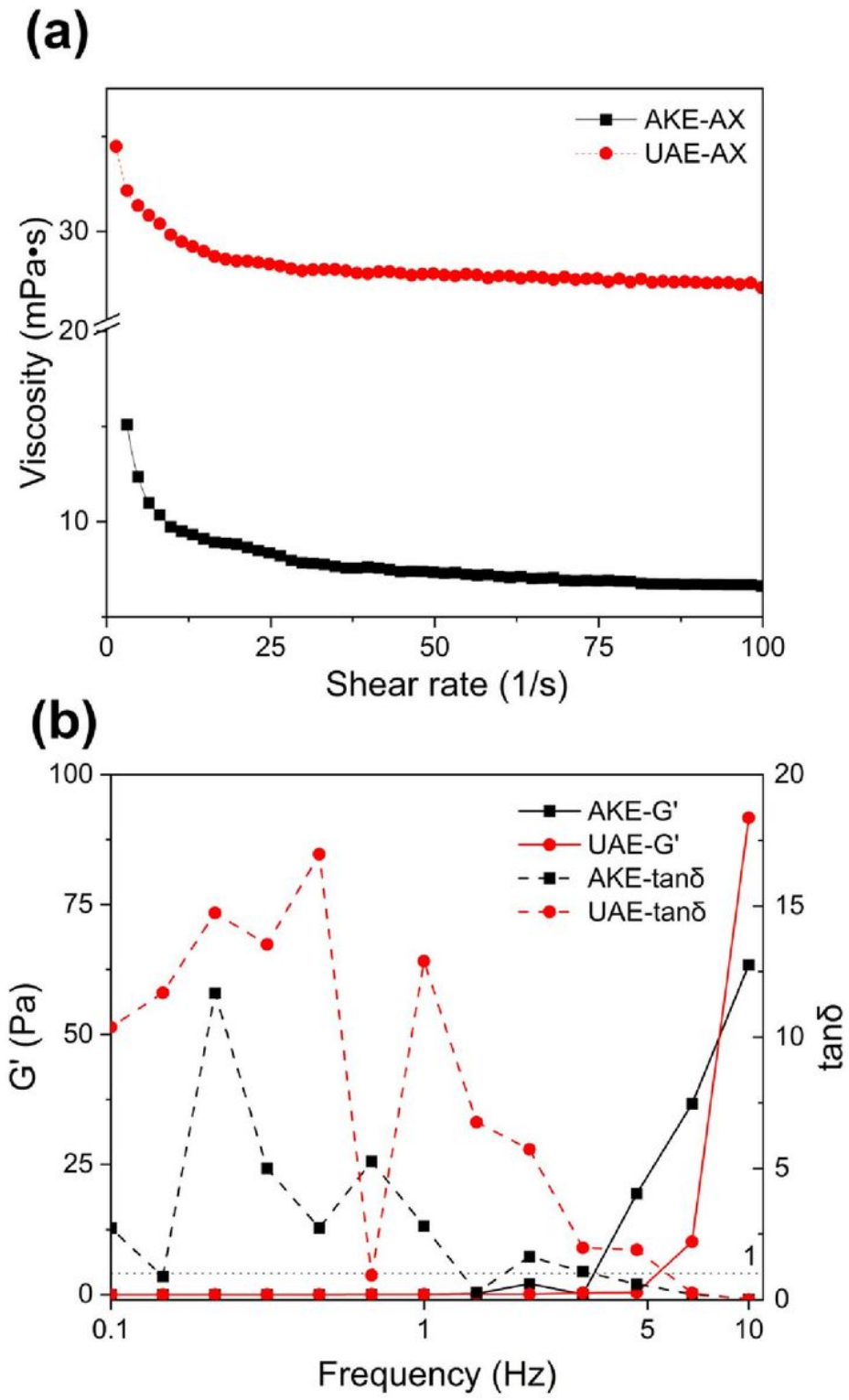


**Figure 4**

(a) apparent viscosity and (b) viscoelasticity of 2% (w/v) aqueous AKE-AX and UAE-AX solution

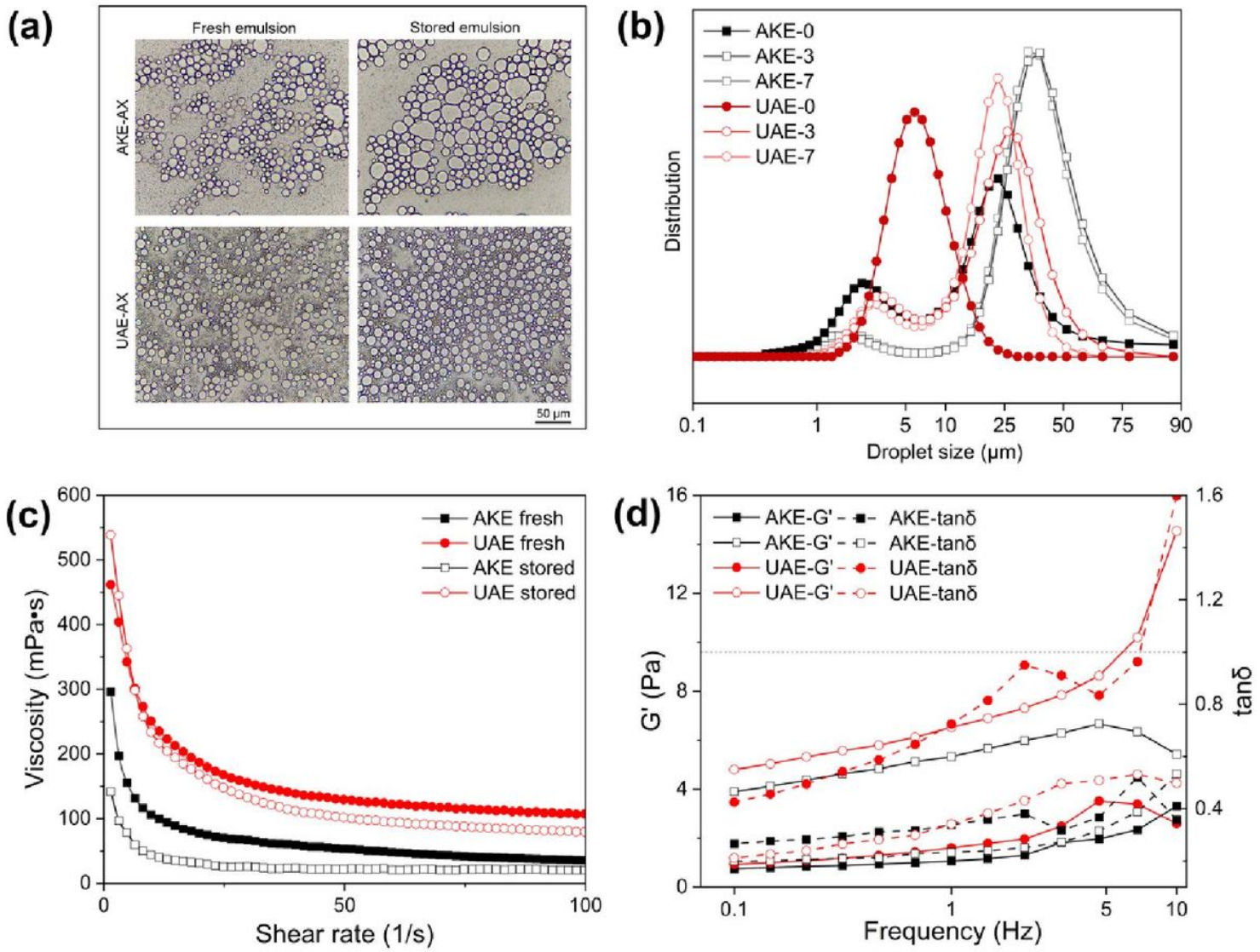


## Figure 5

(a) Apparent viscosity, (b) viscoelasticity and (c) microscope images of fresh and stored emulsions; (d) Droplet size distribution of AKE and UAE emulsion stored for different times (0 day, 3 days, 7 days). Fresh and stored emulsions were represented with filled circles/ boxes and empty circles/ boxes, respectively

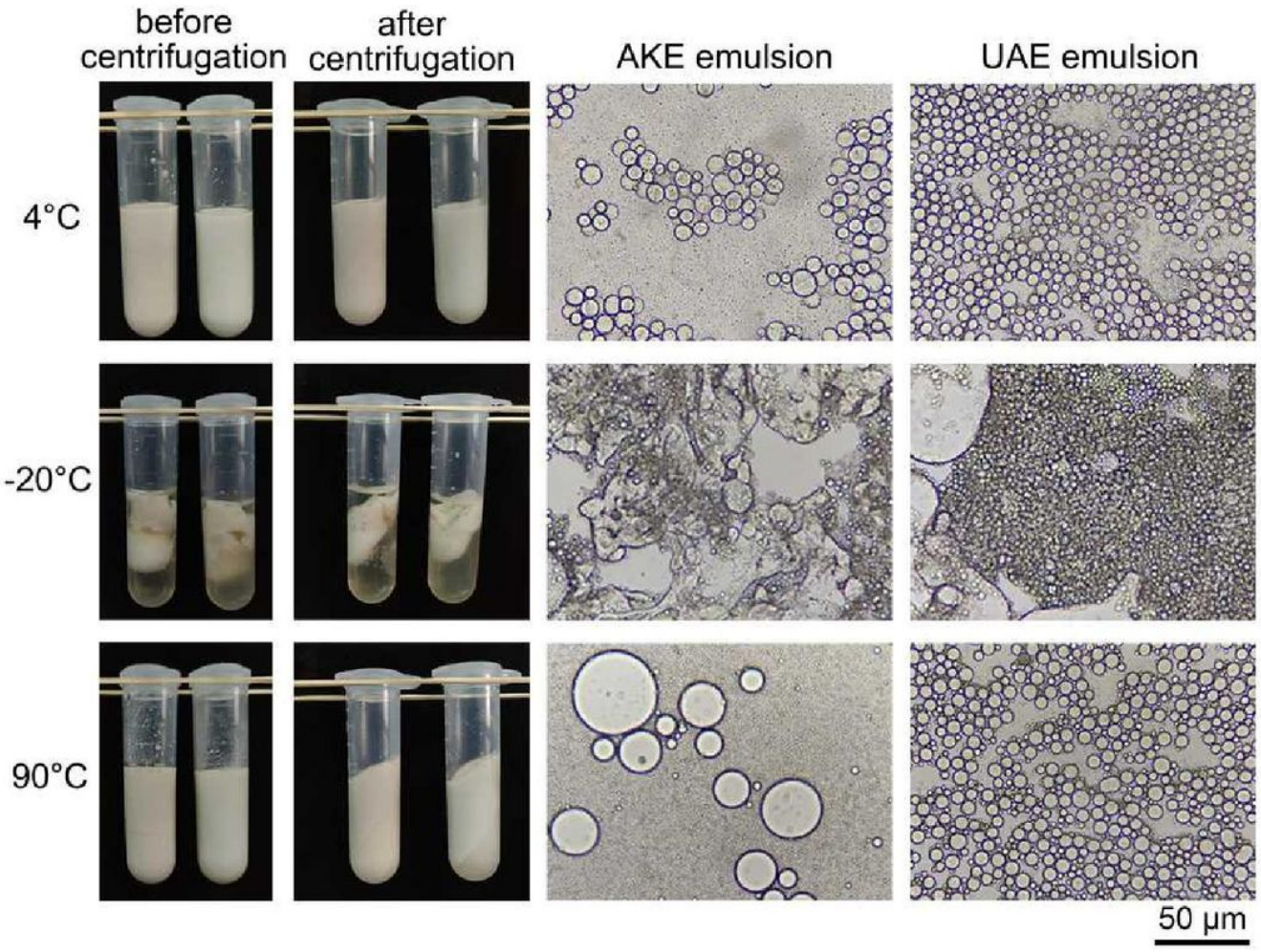


## Figure 6

Appearances and microscope images of AKE (left) and UAE (right) emulsions stored under different conditions